



HAL
open science

Equilibrium Signaling: Molecular Communication Robust to Geometry Uncertainties

Bayram Cevdet Akdeniz, Malcolm Egan, Bao Quoc Tang

► **To cite this version:**

Bayram Cevdet Akdeniz, Malcolm Egan, Bao Quoc Tang. Equilibrium Signaling: Molecular Communication Robust to Geometry Uncertainties. 2020. hal-02536318v1

HAL Id: hal-02536318

<https://hal.science/hal-02536318v1>

Preprint submitted on 8 Apr 2020 (v1), last revised 5 Aug 2020 (v2)

HAL is a multi-disciplinary open access archive for the deposit and dissemination of scientific research documents, whether they are published or not. The documents may come from teaching and research institutions in France or abroad, or from public or private research centers.

L'archive ouverte pluridisciplinaire **HAL**, est destinée au dépôt et à la diffusion de documents scientifiques de niveau recherche, publiés ou non, émanant des établissements d'enseignement et de recherche français ou étrangers, des laboratoires publics ou privés.

Equilibrium Signaling: Molecular Communication Robust to Geometry Uncertainties

Bayram Akdeniz, Malcolm Egan and Bao Quoc Tang

Abstract—A basic property of any diffusion-based molecular communication system is the geometry of the enclosing container. In particular, the geometry influences the system’s behavior near the boundary and in all existing modulation schemes governs receiver design. However, it is not always straightforward to characterize the geometry of the system. This is particularly the case when the molecular communication system operates *in vitro*, where the geometry may be complex or dynamic. In this paper, we propose a new scheme—called *equilibrium signaling*—which is robust to uncertainties in the container geometry. In particular, receiver design only depends on the relative volumes of the transmitter or receiver, and the entire container. Our scheme relies on reversible reactions in the transmitter and the receiver, which ensure the existence of an equilibrium state into which information is encoded. In this case, we derive near optimal detection rules and develop a simple and effective estimation method to obtain the container volume. We also show that equilibrium signaling can outperform classical modulation schemes, such as concentration shift keying, under practical sampling constraints imposed by biological oscillators.

I. INTRODUCTION

The design of diffusion-based molecular communications is heavily dependent on the geometry of the enclosing container. This is due to the fact that the geometry has an important influence on the diffusion of molecules within the container, and determines the statistics for the number of molecules that are observed by a receiver.

The importance of the container geometry is clear in the large body of existing work developing detection schemes for diffusion-based molecular communication systems based on modulation of concentration [1]–[7], [7]–[11], commonly known as concentration shift keying (CSK). Other variations include molecular shift keying [12] and, more recently, reaction shift keying [13]. In these previous works, the detection rules depend heavily on the choice of container geometry, which determines the boundary conditions for the underlying (stochastic) differential equations governing diffusion.

It is not clear that it is always reasonable for the container geometry to be well-characterized. For microfluidic systems, the geometry may not be perfectly known due to the challenges or precisely fabricating micro- or nano-scale channels [14], [15]. On the other hand, *in vitro* molecular communications—such as in or between cells—may occur in environments which are difficult to characterize [16]. Even if the geometry is known, it may be too complicated to accurately derive the resulting channel response. It is therefore desirable to seek

signaling strategies that are not geometry-dependent. That is, modulation schemes that induce receiver observations that are robust to changes in the geometry.

In this paper, we propose a new signaling scheme for which the receiver observations only depend on the transmitted signals and the total volume of the container and not on the specific geometry. Our scheme relies on systems of chemical reactions within both the transmitter and the receiver. That is, the receiver is also capable of producing information-carrying molecules. Under a variety of conditions—typically requiring the presence of reversible chemical reactions—the quantity of molecules in the receiver then converges to an equilibrium state [17], independent of the specific geometry of the container. When the equilibrium state can be accurately characterized, reliable communication can be supported.

For our signaling scheme—which we call *equilibrium signaling*—it is feasible to analytically derive near-optimal detection rules for a wide range of container geometries. For example, such near-optimal detection rules are feasible for the containers in Fig. 1. For other modulation schemes, such as classical CSK, the optimal detection rule in the case of the examples in Fig. 1 would require numerical solution of a partial differential equation. We remark that this remains true also for the reactive signaling schemes proposed in [18], [19].

One potential challenge in exploiting the equilibrium state to communicate is a low sampling rate. This is due to the need to wait until the system approaches an equilibrium state after each transmission. Nevertheless, for many proposed applications of molecular communications, biochemical circuits are highly desirable. At present, biochemical oscillators typically have a period on the order of, at least, minutes [20]. Since the sampling rate depends on the period of the oscillator, sampling near the equilibrium state may not only be desirable but also necessary.

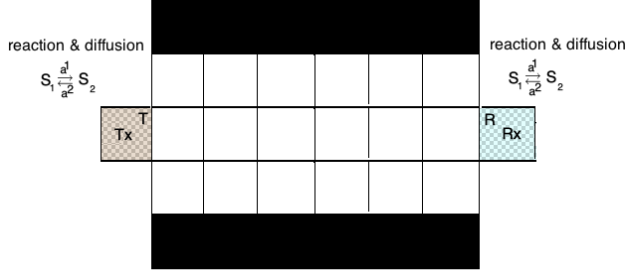
In principle, a vast number of chemical reaction-diffusion systems can provide the equilibrium state required for equilibrium signaling. However, the key challenge is to obtain a precise characterization of the statistics for receiver observations, which is in general an open problem. To this end, we primarily focus on molecular communication systems involving a single reversible unimolecular (or first-order) reaction. Nevertheless, systems involving larger numbers of unimolecular reactions satisfying generalized reversibility conditions can also be realized. Appropriately interpreted, such a class of reactions is able to model a wide range of chemical dynamics [21].

Allowing for spatially inhomogeneous diffusion, we obtain an accurate approximation for the receiver observations. This is justified both through analytical approximation and

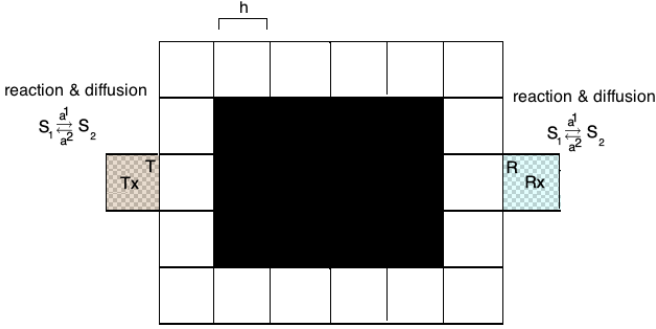
B. Akdeniz and M. Egan are with Université de Lyon, INSA Lyon, INRIA, CITI, France. B.Q. Tang is with Institute of Mathematics and Scientific Computing, University of Graz, Austria

TABLE I: Notation.

Variable	Definition
N	Number of voxels in the system.
V_{vox}	Volume of each voxel.
$V_{\text{Tx}}, V_{\text{Rx}}$	Volume of the transmitter and receiver.
S_1, S_2	Chemical species.
$\mathbf{M}_i(t) = [M_i^1(t), M_i^2(t)]$	State vector of voxel i in time t .
κ_{ij}^l	Diffusive jump rate.
$a_j^l, l = 1, 2.$	Reaction rate constants.
ν_j^k	Quantity of each species k produced or removed in reaction j .
$N_{\text{Rx},j}(t)$	Number of S_j molecules in the receiver at time t .
S_n^m	Binary sequence with length n and m elements bit 1.
s_k	k -th symbol of S_n^m .
T_s	Communication time interval.
Δ	Number of transmitted molecules for each bit 1 transmission.
μ_r	Expected number of molecules in the receiver of S_1 for a transmission of bit 1.
$D_l(\mathbf{x}), l = 1, 2.$	Spatially dependent diffusion coefficient.



(a) A 2-D channel (molecules cannot diffuse into the black region).



(b) A 2-D channel (molecules cannot diffuse into the black region).

Fig. 1: Containers with complex geometry.

empirical statistical analysis. Under this approximation, we derive the optimal detection rule. However, this rule requires the use of a variant on Viterbi decoding and hence requires storage of all previous observations of the receiver, which may be problematic for biological circuit implementations. To obtain a computationally feasible solution, we also introduce a suboptimal scheme based on a heuristic decision rule based on the difference between the last two observations.

We then focus on system parameter design, including the sampling time and optimal decision threshold—in terms of the symbol error rate—for the computationally feasible suboptimal scheme. We also introduce a simple method to estimate the container volume, accounting for the increase of molecules in the system due to pilot transmissions.

Unlike classical CSK schemes, equilibrium signaling is robust to the container geometry. In particular, classical CSK schemes are highly dependent on effective distance estimation in addition to container boundaries. On the other hand, equilibrium signaling is only dependent on the volume of the container. We also find that our scheme significantly outperforms classical CSK in the presence of reversible reactions and the same sampling rate.

II. SYSTEM MODEL

Let $\Omega \subset \mathbb{R}^d$, $d \in \{1, 2, 3\}$ be a domain with smooth boundary $\partial\Omega$ consisting of transmitting and receiving devices with a fluid medium separating the devices. Consider the

discretization of Ω into N volume elements (voxels) each of volume V_{vox} , with the set of points in voxel i denoted by \mathcal{V}_i , $i = 1, \dots, N$. Here, volume is interpreted as length in \mathbb{R}^1 , area in \mathbb{R}^2 , and volume in \mathbb{R}^3 .

Messages to be sent by the transmitter with volume V_{Tx} are encoded into the quantity of species S_1 . Within the transmitter and the receiver, each species is produced or removed via the unimolecular reactions



In particular, the transmitter produces information-carrying molecules of species S_2 by the first reaction in (1).

Considering unimolecular reactions is not as restrictive as it may appear. In particular, unimolecular reactions are capable of modeling the dynamics of a range of biochemical systems [21]. We assume that molecules of species S_1 produced in the transmitter are not capable of diffusing into the channel. On the other hand, this is possible for species S_2 .

At the receiver, with volume V_{Rx} (not necessarily the same as V_{Tx}), molecules of species S_2 are able to generate molecules of species S_1 via the second reaction in (1). The receiver can then attempt to decode the transmitted message based on observations of the quantities of species S_1 and species S_2 that are present at the sampling time.

In order to capture the effect of small quantities of each chemical species in the system, we consider a stochastic model for the kinetics. To formally describe the scenario, we introduce the following notation. Let $M_i^l(t)$, $l = 1, 2$, $i = 1, \dots, N$ denote the random variable for the number of molecules of species S_1 or S_2 in voxel i at time t . Denote $\mathbf{M}_i(t) = [M_i^1(t), M_i^2(t)]$ as the state vector in voxel i and the matrix $\mathbf{M}(t) = [\mathbf{M}_1(t), \dots, \mathbf{M}_N(t)]$. The probability that $\mathbf{M}(t)$ has value \mathbf{m} at time t is then denoted by

$$P(\mathbf{m}, t) = \Pr(\mathbf{M}(t) = \mathbf{m} | \mathbf{M}(0) = \mathbf{m}_0), \quad (2)$$

where $\mathbf{M}(0)$ is the initial quantity of molecules of each species in each voxel.

Since each reaction is unimolecular, it follows that in each reaction the number of molecules of the two species involved can only increase or decrease by one. Let $\mathbf{1}_i^l$ be the state where the number of molecules in all voxels is zero, except for species l in voxel i . That is, $\mathbf{M}(t) + \mathbf{1}_i^l$ means that the number of molecules of species l in voxel i is increased by one.

A popular model for stochastic kinetics of molecules is the reaction-diffusion master equation [22], also utilized in the context of molecular communications in [23]. In this model, the diffusive jump rate is denoted by κ_{ij}^l for each individual molecules of the l -th species moving from voxel j into voxel i , with $\kappa_{ii} = 0$, $i = 1, \dots, N$. In particular, the probability per unit time that a molecule of S_l diffuses from voxel j to voxel i at time t is given by $\kappa_{ij}^l M_j^l(t)$.

In general, κ_{ij}^l depends on i, j and l ; that is, the probability of a molecule diffusing between two voxels is not spatially homogeneous (diffusive jump rates vary from voxel to voxel). While spatially homogeneous diffusion is a standard assumption in the molecular communications literature, variations in the fluid environment can induce inhomogeneity which we are able to capture within our model.

We remark that an alternative stochastic model has recently been studied in the context of reactive signaling [18]. A key feature of the RDME model is that it provides information about the statistical dependence in the receiver observations over time, which is not the case for [18]. We also note that spatial homogeneity for the diffusion process is assumed in [18] and in the vast majority of other work on molecular communications.

In the case of mass-action kinetics and first-order reactions, the probability per unit time that a molecule of S_l in voxel i reacts at time t is given by $a_i^l M_i^l(t)$ with rate constants a_i^l . In general, the reaction rate is dependent on the voxel index. The net change of each chemical species due to the reaction with substrate S_l is expressed via the column vector $\boldsymbol{\nu}_l \in \mathbb{N}^2$. The term $\boldsymbol{\nu}_l \mathbf{1}_i$ indicates that $\mathbf{M}(t)$ changes by $\boldsymbol{\nu}_k$ in the i -th voxel.

Remark 1. *In order to model production of S_1 in the transmitter and S_2 , we assume that for voxels i comprising the transmitter and the receiver $a_i^1 = a^1$, while $a_i^1 = 0$ for voxels comprising the channel.*

In the RMDE model, the probability distribution $\Pr(\mathbf{m}, t)$ evolves according to the system of differential equations given by

$$\begin{aligned} & \frac{dP(\mathbf{m}, t)}{dt} \\ &= \sum_{i=1}^N \sum_{j=1}^N \sum_{l=1}^2 (\kappa_{ij}^l (m_j^l + 1) P(\mathbf{m} + \mathbf{1}_j^l - \mathbf{1}_i^l, t) \\ & \quad - \kappa_{ji}^l m_i^l P(\mathbf{m}, t)) + \sum_{i=1}^N \sum_{l=1}^2 (a_i^l (m_i^l + 1) P(\mathbf{m} - \boldsymbol{\nu}_l \mathbf{1}_i, t) \\ & \quad - a_i^l m_i^l P(\mathbf{m}, t)). \end{aligned} \quad (3)$$

The system of ordinary differential equations in (3) corresponds to the Kolmogorov forward equation for a continuous-

time Markov chain; that is, the evolution of the system state is Markovian. In our setting, the Markov chain corresponding to the RDME is irreducible and positive recurrent. Therefore, a stationary distribution exists and is given by [24]

$$\pi(\mathbf{m}) = \lim_{t \rightarrow \infty} \Pr(\mathbf{M}(t) = \mathbf{m} | \mathbf{M}(0) = \mathbf{m}_0). \quad (4)$$

III. PROPOSED EQUILIBRIUM SIGNALING STRATEGY

The existence of an equilibrium state provides the opportunity to develop a new signaling strategy. In particular, if the statistics for the quantity of each species at the receiver can be characterized, transmitted symbols may be recovered based on observations within the equilibrium state. As we will show, such an approach is highly robust to uncertainties in the container geometry, which is not the case for classical CSK signaling schemes.

In this section, we detail our proposed equilibrium signaling strategy tailored to the model in Section II. We focus on the case of binary signaling; that is, for the transmitter to send a bit 1, it generates Δ molecules of species S_1 within a single voxel of the transmitter. For the case of bit 0, the transmitter generates zero molecules of species S_1 . Each bit is equally likely to be sent.

Assume that the system operates using time slots with duration T_s and that no molecules of species S_1 nor S_2 are present in the system at $t = 0$. The bit to be transmitted in time slot n is denoted by s_n . Moreover, molecules that are produced by the transmitter may change the number of each species via the reactions in (1); however, no molecules degrade.

Consider the n -th time slot. Due to the previous $n - 1$ transmissions, there are $N_{\text{Tx},l}(nT_s)$, $l = 1, 2$ molecules of species S_l in the transmitter. At a time $nT_s + \delta$ shortly after the beginning of the time slot, the transmitter produces a quantity of S_1 depending on the bit to be transmitted. In particular,

$$N_{\text{Tx},1}(nT_s + \delta) = \begin{cases} N_{\text{Tx},1}(nT_s) + \Delta & s_n = 1, \\ N_{\text{Tx},1}(nT_s) & s_n = 0, \end{cases} \quad (5)$$

for $\delta > 0$ a sufficiently small period of time; that is, δ is chosen such that no reactions occur nor any molecules diffuse to a voxel outside of the transmitter.

The key idea behind the proposed signaling strategy is that for sufficiently large T_s , the total number of molecules of species S_1 and S_2 in the receiver at the time of sampling will be approximately drawn from the stationary distribution of the RDME. As such, if the stationary distribution is known, then near-optimal detection rules can be obtained.

To this end, suppose that a sequence of bits, s_1, \dots, s_n , over a period of n sampling intervals is sent. Let S_n^m denote such a sequence containing with m transmissions (each corresponding to a bit 1). Further, let $N_{\text{Rx},1}(nT_s | S_n^m)$ denote the number of molecules of species S_1 observed by the receiver at the end of the n -th symbol period (i.e., at time $(n + 1)T_s$), given the transmitted sequence S_n^m .

We make the following assertion, which will be validated in Section IV.

Assertion 1.

$$N_{\text{Rx},1}(nT_s | S_n^m) \sim \mathcal{N}(m\mu_r, m\mu_r), \quad (6)$$

where $\mu_r > 0$ is a known constant, only dependent on the volume of the enclosing container and not the specific geometry, and $\mathcal{N}(\mu, \sigma^2)$ denotes the Gaussian law with mean μ and variance σ^2 . In particular,

$$\mu_r = \frac{\Delta \frac{V_{\text{Rx}}}{NV_{\text{vox}}}}{1 + \frac{a^1 V_{\text{Tx}} + V_{\text{Rx}}}{a^2 NV_{\text{vox}}}}. \quad (7)$$

Under the assumption that $a^1 = a^2$ and $V_{\text{Tx}} = V_{\text{Rx}}$,

$$\mu_r = \frac{\Delta V_{\text{Rx}}}{NV_{\text{vox}} + 2V_{\text{Rx}}}. \quad (8)$$

In (6), μ_r is the average number of molecules for each species in each voxel given Δ molecules are in the system (corresponding to a single transmission of bit 1). To gain some intuition into the value of μ_r , consider the case when $a^1 = a^2$ and $V_{\text{Rx}} = V_{\text{Tx}}$. Recall that the effect of diffusion is to evenly spread the molecules of each species between all voxels. This implies that the number of molecules of S_1 is the same within each voxel comprising \mathcal{V}_{Tx} and \mathcal{V}_{Rx} . Moreover, the number of molecules of S_2 is the same within each voxel in the total volume. On the other hand, the effect of the reactions is to produce, on average at equilibrium, the same number of molecules of each species within the transmitter and receiver voxels. As such on average at equilibrium, there are twice the total number of molecules in the transmitter and receiver voxels compared with the voxels comprising the channel.

Under Assertion 1, the distribution for the quantity of S_1 in the receiver at the sampling time for the $n + 1$ -th time slot, corresponding to a transmission $s_{n+1} \in \{0, 1\}$ is given by

$$N_{\text{Rx},1}((n+1)T_s | S_n^m, s_{n+1}) \sim \begin{cases} \mathcal{N}(m\mu_r, m\mu_r) & s_{n+1} = 0, \\ \mathcal{N}((m+1)\mu_r, (m+1)\mu_r) & s_{n+1} = 1. \end{cases} \quad (9)$$

A. Near-Optimal Detection

We seek to obtain an estimate for the sequence (s_1, \dots, s_{n+1}) . Although the observation process is Markovian, for a sufficiently large time slot T_s , the observations $N_{\text{Rx},1}(T_s), \dots, N_{\text{Rx},1}((n+1)T_s)$ are approximately independent. Let $\mathbf{N}_{\text{Rx},1}$ denote the vector of observations at the receiver for the quantity of S_1 and $\mathbf{s} \in \{0, 1\}^{n+1}$ denote a potential vector of transmitted bits. Under Assertion 1, the joint likelihood of the observations is given by

$$f_{\mathbf{N}_{\text{Rx},1}|\mathbf{s}}(\mathbf{n}) = \prod_{i=1}^{n+1} \frac{1}{\sqrt{2\pi\mu_r \sum_{j=1}^i s_j}} \exp\left(-\frac{(n_i - \mu_r \sum_{j=1}^i s_j)^2}{2\mu_r \sum_{j=1}^i s_j}\right), \quad (10)$$

and, assuming the independence of elements of $\mathbf{N}_{\text{Rx},1}$, the optimal detection rule is given by

$$\hat{\mathbf{s}}^* = \arg \max_{\mathbf{s} \in \{0,1\}^{n+1}} f_{\mathbf{N}_{\text{Rx},1}|\mathbf{s}}(\mathbf{n}). \quad (11)$$

A brute force search for the estimate $\hat{\mathbf{s}}^*$ in (10) leads to a complexity that grows exponentially in n . Nevertheless, the Viterbi algorithm with appropriate branch weights can be used

to solve the optimization problem with complexity of order $O(n)$. Note that while the Viterbi algorithm yields an optimal solution for (11), it is under the assumption that Assertion 1 holds.

We briefly sketch the computations in Algorithm 1, which is a form of the Viterbi algorithm with branch metrics tailored to the problem in (10). For the k -th symbol $s_k \in \{0, 1\}$, let $p(n_k | s_k) = \log(f_{N_{\text{Rx},1}(kT_s)|s_k}(n_k))$. In the k -th symbol interval, it is necessary to compute $P_{k-1,0}$ and $P_{k-1,1}$, which correspond to the probability of the most probable sequence until the $k - 1$ -th symbol and the k -th symbol is 0 and 1, respectively.

Algorithm 1 Near-Optimal Detection Algorithm

- 1: **Input:** $s_k \in \{0, 1\}$, $p(n_k | s_k)$,
 - 2: for $k = 1$ to $n + 1$
 - $\log P_{k,0} = \max(\log P_{k-1,0} + p(n_k|0), \log P_{k-1,1} + p(n_k|0))$.
 - $\log P_{k,1} = \max(\log P_{k-1,0} + p(n_k|1), \log P_{k-1,1} + p(n_k|1))$.
 - $s_{k,0} = \arg \max_{i,j} \log P_{k,i}$.
 - $s_{k,1} = \arg \max_{i,j} \log P_{k,i}$.
 - 3: Find the most probable path:
 - $u = \arg \max_i P_{n+1,i}$.
 - 4: Backtrack this path:
 - $\hat{\mathbf{s}}^* = \{s_{1,u}, s_{2,u}, \dots, s_{n+1,u}\}$.
-

B. Detection with Low Memory Requirements

For large n , directly solving the optimization problem in (11) requires the storage all previous observations, which may not be feasible due to limitations of the underlying biological circuits. As such, it also is desirable to consider approaches that only require limited memory.

To this end, define

$$R(n+1) = N_{\text{Rx},1}((n+1)T_s) - N_{\text{Rx},1}(nT_s). \quad (12)$$

In this case, each bit is decoded sequentially via the detection rule

$$\tilde{s}_{n+1} = \begin{cases} 1 & R(n+1) > \tau, \\ 0 & \text{otherwise.} \end{cases} \quad (13)$$

The optimal choice of τ for the decision rule in (13) can be obtained via an analysis of the bit error rate, which we carry out in Section V-B. As will be shown in Section VI-A via particle-based simulations, this low memory detection achieves nearly the same performance as the near-optimal algorithm in Algorithm 1.

IV. EQUILIBRIUM CHARACTERIZATION: JUSTIFICATION OF ASSERTION 1

The potential of the signaling scheme in Section III relies on the validity of Assertion 1. We first develop a stochastic linear noise approximation of the RDME model in Section II, which justifies the Gaussian law. We then perform the Kolmogorov-Smirnov test to provide a further empirical validation.

A. Stochastic Linear Noise Approximation

It is known that for stochastic chemical reaction networks under mass-action kinetics, the evolution of the molecular counts of each species can be approximated by the chemical Langevin equation [25]. Since diffusion is modeled by unimolecular reactions in the RDME model in Section II, it follows that a similar approximation can be applied. In particular, we have

$$\begin{aligned}
M_i^l(t + \tau) &\approx M_i^l(t) + \sum_{j=1}^N \kappa_{ij}^l M_j^l(t) \tau + \sum_{j=1}^N \sqrt{\kappa_{ij}^l M_j^l(t)} \tau \mathcal{N}_{D,j}(0, 1) \\
&\quad - \sum_{j=1}^N \kappa_{ji} M_i^l(t) + \sum_{j=1}^N \sqrt{\kappa_{ji}^l M_i^l(t)} \tau \mathcal{N}_{D',j}(0, 1) \\
&\quad + a_i^{3-l} M_i^{3-l}(t) \tau - a_i^l M_i^l(t) \tau \\
&\quad + \sum_{k=1}^2 \sqrt{a_i^k M_i^k(t)} \tau \mathcal{N}_{R,k}(0, 1), \tag{14}
\end{aligned}$$

where each standard normal random variable $\mathcal{N}_{D,j}(0, 1)$, $\mathcal{N}_{D',j}(0, 1)$, and $\mathcal{N}_{R,k}(0, 1)$ are independent.

Let $V = V_i$, $i = 1, \dots, N$ be the volume of voxel i and define the concentration of species S_l in voxel i by

$$C_i^l(t) = \frac{M_i^l(t)}{V}. \tag{15}$$

It then follows from the RDME that

$$\begin{aligned}
\frac{d\mathbb{E}[C_i^l(t)]}{dt} &= \sum_{j=1}^N (\kappa_{ij}^l \mathbb{E}[C_j^l(t)] - \kappa_{ji}^l \mathbb{E}[C_i^l(t)]) \\
&\quad - \mathbb{E}[a_i^l C_i^l(t)] + \mathbb{E}[a_i^{3-l} C_i^{3-l}(t)], \tag{16}
\end{aligned}$$

which follows from [22, Sec. 1.1.3].

Since all reactions are unimolecular, under the assumption that the diffusion jump rates, κ_{ij} , are chosen appropriately, the expected concentrations converge to a deterministic reaction-diffusion system [22]. In particular, let u_1, u_2 be the deterministic concentrations. Then, the deterministic system is described by the system of partial differential equations, for all $l = 1, 2$,

$$\begin{cases} \partial_t u_l - \operatorname{div}(D_l(\mathbf{x}) \nabla u_l) = a^{3-l}(\mathbf{x}) u_{3-l} - a^l(\mathbf{x}) u_l, & \mathbf{x} \in \Omega, \\ D_l(\mathbf{x}) \nabla u_l \cdot \nu = 0, & \mathbf{x} \in \partial\Omega, \\ u_l(\mathbf{x}, 0) = u_{l0}(\mathbf{x}), & \mathbf{x} \in \Omega, \end{cases} \tag{17}$$

where ∂_t denotes the derivative with respect to time. The vector-valued function $\nu(\mathbf{x})$ is the outer unit normal defined for $\mathbf{x} \in \partial\Omega$. The condition $D_l(\mathbf{x}) \nabla u_l \cdot \nu = 0$ is a homogeneous Neumann boundary condition. The initial data u_l , $l = 1, 2$, is assumed to be nonnegative. The diffusion coefficients satisfy $D_l(\mathbf{x}) \geq 0$ and can be zero on a set with positive measure. For spatially homogeneous diffusion coefficients $D_l(\mathbf{x}) = D_l$, $\mathbf{x} \in \Omega$.

Using the same argument as [26], it follows from the Langevin approximation in (14) that fluctuations are of the order of \sqrt{V} . This suggests the Gaussian approximation

$$M_i^l(t) \approx V u_l(\mathbf{x}_i, t) + \sqrt{V} Z_i^l(t), \tag{18}$$

where $Z_i^l(t)$ is a zero-mean Gaussian random variable and \mathbf{x}_i is a point inside the i -th voxel. We note that this approximation can be rigorously justified in the case of chemical reaction networks [26] via a convergence result in [27]. A similar result for the reaction-diffusion setting with spatially homogeneous diffusion and reactions is available in [28].

B. Verification of Assertion 1

The linear noise approximation provides a justification for the Gaussianity of the stationary distribution required to establish Assertion 1. However, the mean and the variance are dependent on the equilibrium solution to the system of PDEs in (17). At present, for the spatially inhomogeneous reaction rates and diffusion coefficients, even the existence of an equilibrium solution has not been rigorously established.

Nevertheless, the ansatz for the mean and variance of the stationary distribution in Assertion 1 is provided for the related problem where only the diffusion coefficients are spatially inhomogeneous; that is, the reaction rates are spatially homogeneous or, said in different words, independent of the spatial coordinates. In this case, it has been established in [29] that the mean and variance do indeed correspond to those given in Assertion 1.

To empirically validate the ansatz, we have carried out Monte Carlo simulations and performed a Kolmogorov-Smirnov test. Both a standard 2-D scenario and a non-standard 2-D scenario are considered, illustrated in Fig. 2a and Fig. 2b, respectively. In the numerical validation, the following parameters are used: $a^1 = a^2 = 1$, $\Delta = 600$, $V_{\text{Rx}} = V_{\text{Tx}} = V_{\text{vox}} = 10^{-6}$, $N \in \{60, 100\}$, $D_l(\mathbf{x}) = D_l \in \{4, 40, 400\} \times 10^{-9}$, $\mathbf{x} \in \Omega$, the corresponding diffusive jump rates $\kappa_{ij}^l = D_l/h^2$ for cubic voxels with height h [22].

The first step is to verify that the deterministic system of differential equation in (17) admits a spatially homogeneous solution as the time $t \rightarrow \infty$. To do so, we obtain a numerical solution using the method in [30], for a range of different system parameters.

To verify that the mean quantity of molecules is consistent with Assertion 1, we estimate the mean from a particle-based simulation. In Fig. 3, there are $N = 60$ voxels and $\Delta = 600$ molecules in the system. In the voxels of the transmitter and the receiver, both S_1 and S_2 are present. Moreover, since the reactions $a^1 = a^2$, the expected number of molecules at the equilibrium for each voxel is equal to $\frac{600}{60+2} = 9.68$, which is consistent with Fig. 3. In Fig. 4, we examine the scenario where the diffusion coefficient is spatially inhomogeneous and again observe spatial homogeneity of the equilibrium. Here, $N = 100$ and hence the expected number of molecules at the equilibrium for each voxel is equal to $\frac{600}{100+2} = 5.88$.

In order to verify that the number of observed molecules is well approximated by the Gaussian law in Assertion 1, we perform the Kolmogorov-Smirnov test based on particle-based simulations of the system. In the Kolmogorov-Smirnov test, $H(t)$ denotes the empirical distribution function (estimated from the simulated data) and $F(t)$ denotes the candidate distribution function (given in Assertion 1). The Kolmogorov-Smirnov statistic between two distributions is

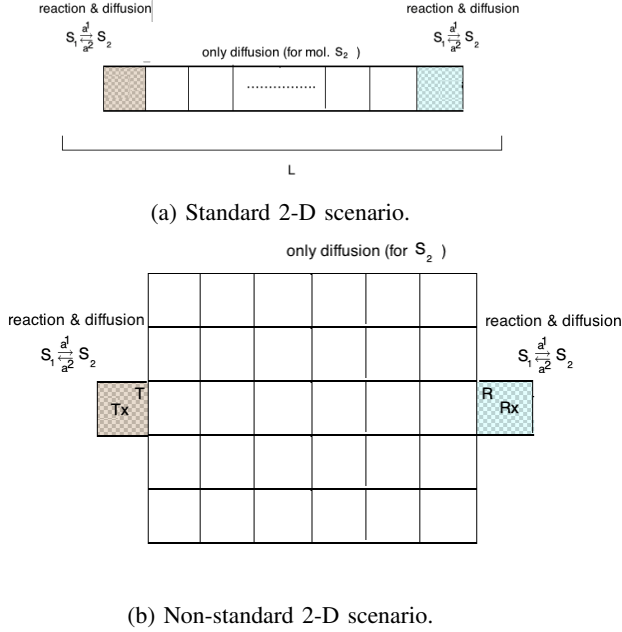


Fig. 2: Miscellaneous channel models

TABLE II: KS Test for Assertion 1.

Parameters	Acceptance Probability	p -value
$\Delta = 60, NV_{\text{vox}}/V_{\text{Rx}} = 10$	0.92	0.32
$\Delta = 100, NV_{\text{vox}}/V_{\text{Rx}} = 10$	0.93	0.40
$\Delta = 600, NV_{\text{vox}}/V_{\text{Rx}} = 10$	0.94	0.46
$\Delta = 100, NV_{\text{vox}}/V_{\text{Rx}} = 20$	0.92	0.40
$\Delta = 600, NV_{\text{vox}}/V_{\text{Rx}} = 20$	0.92	0.43
$\Delta = 600, NV_{\text{vox}}/V_{\text{Rx}} = 100$	0.91	0.43

then given by $T^* = \sup_t (|H(t) - F(t)|)$. The hypothesis that the candidate distribution is true is rejected if

$$\alpha > 1 - F_{\text{Kol}}(\sqrt{UT}^*), \quad (19)$$

where $\alpha \in (0, 1)$ is the significance level ($\alpha \approx 0$ corresponds to high significance), U is the number of samples, and F_{Kol} is the distribution function of Kolmogorov distribution [31].

In our setting, we compare the observations at the receiver with the Gaussian law in Assertion 1 using the Kolmogorov-Smirnov test for $U = 500$. Table II shows the results of the test with a confidence of $\alpha = 0.05$. As can be seen in this table, data obtained from the particle-based simulations is in good agreement Assertion 1 with high acceptance rate and p -values significantly larger than the confidence level $\alpha = 0.05$, which suggests that Assertion 1 cannot be ruled out.

V. SYSTEM PARAMETER DESIGN

In this section, we focus on the design of key system parameters including the sampling time, the detection threshold in the low memory scheme from Sec. III-B. We also develop an estimation procedure for the container volume, which is necessary for selecting the decision threshold.

A. Choosing the Sampling Time

The equilibrium signaling scheme is based on the assumption that sampling is performed when the system is nearly in

equilibrium. As such, we now turn to the problem of selecting the sampling time. We base the analysis on the underlying deterministic system in (17), which determines the average behavior of the system governed by the RDME.

As a tractable closed-form solution to (17) is not available, we introduce a heuristic approach which provides a means of selecting the sampling time. The analysis is based on a one dimensional model with a spatially homogeneous diffusion coefficient for S_2 . This is in order to obtain a simple heuristic in order to obtain a sampling time.

Our approach decomposes the kinetics into three phases: a reaction-limited phase in the transmitter; diffusion of S_2 from the transmitter to the receiver; and a reaction-limited phase in the receiver. Each phase is formalized in the following, where we assume $a^1 = a^2 = a$ and $V_{\text{Tx}} = V_{\text{Rx}}$.

a) *Phase A*: In the first phase, the system is modeled as a single container with reaction $S_1 \rightarrow S_2$ and no diffusion. In particular, the initial concentration of S_l is denoted by $u_{A,l}^0$, with $u_{A,1}^0 = \Delta$ and $u_{A,2}^0 = 0$, and the concentrations evolve according the following differential equation

$$\frac{du_{A,1}}{dt} = -au_{A,1}(t), \quad (20)$$

which admits the explicit solution

$$u_{A,1}(t) = u_{A,1}(0)e^{-at} = \Delta e^{-at}. \quad (21)$$

It is clear that $\lim_{t \rightarrow \infty} u_{A,1}(t) = 0$. On the other hand, for sufficiently small ϵ , we can obtain the approximate equilibrium time for the first phase, t_A , by plugging $u_{A,1}(t) = \epsilon$ into (21) as

$$t_A = -\frac{1}{a} \log\left(\frac{\epsilon}{\Delta}\right). \quad (22)$$

b) *Phase B*: In the second phase, a diffusion-limited model is adopted, where chemical reactions are ignored. In this case, the concentration evolves according to

$$\frac{\partial u_{B,2}}{\partial t}(x, t) = D \frac{\partial^2 u_{B,2}}{\partial x^2}(x, t), \quad (23)$$

where $u_{B,2}(x, 0) = \Delta \delta_{x=0}$, with $\delta_{x=0}$ denoting the Dirac delta function. The solution to this differential equation is given by

$$u_{B,2}(x, t) = \frac{\Delta}{\sqrt{4\pi Dt}} \exp\left(-\frac{x^2}{4Dt}\right). \quad (24)$$

Since at equilibrium, spatial homogeneity is required, the spatial derivative in (24) should be negligible. This implies that $L^2 \ll 4Dt$ where L is chosen to be the maximum distance between the transmitter and the container. Therefore, the required time for spatial homogeneity, t_B , can be expressed as

$$\frac{L^2}{4D} \ll t_B. \quad (25)$$

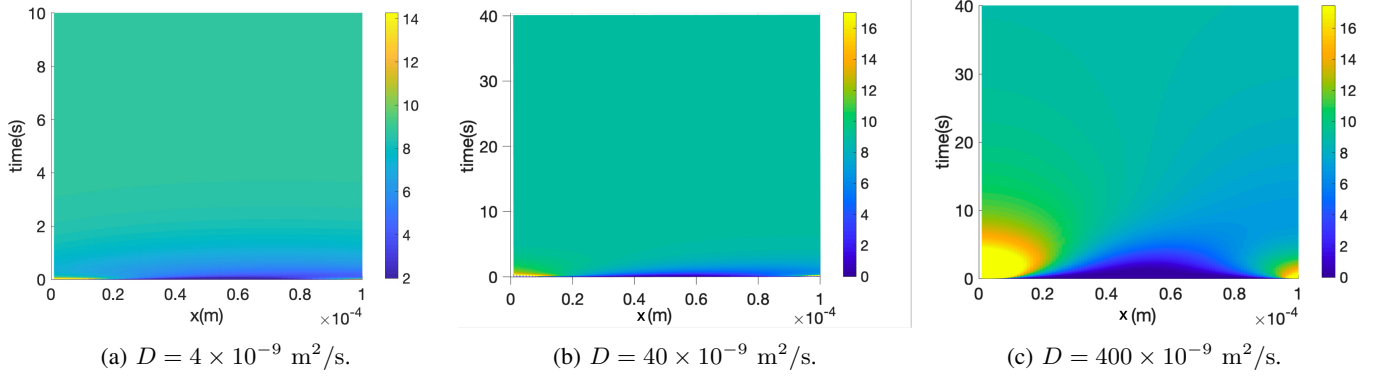


Fig. 3: Solution of (17) for the concentration of S_2 for $a^1 = a^2 = 1 \text{ s}^{-1}$, $\Delta = 600$, $V_{\text{Rx}} = V_{\text{Tx}} = V_{\text{vox}} = 10^{-6}$, $N = 100$, $D = 4, 40, 400 \times 10^{-9}$.

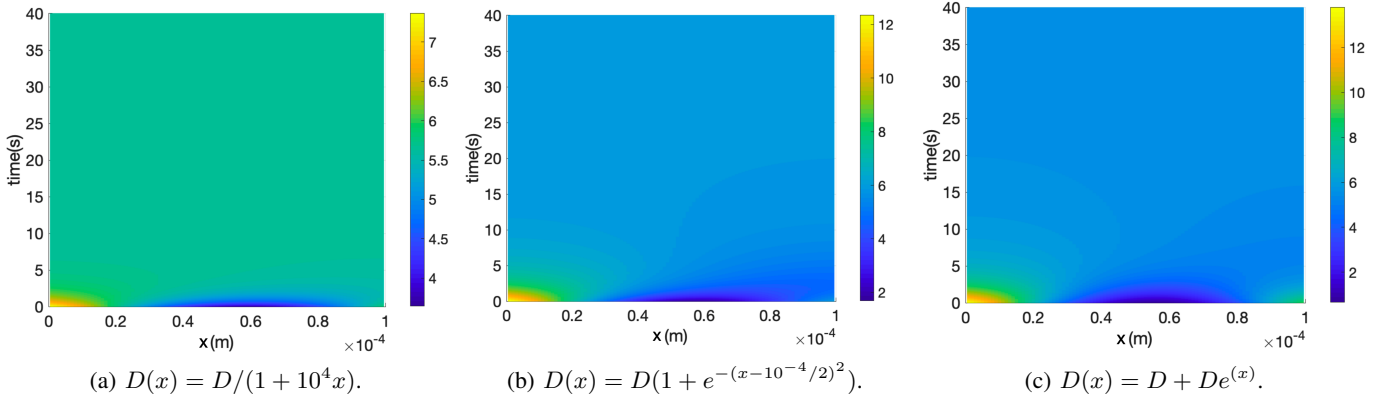


Fig. 4: Solution of (17) for the concentration of S_2 for different $D(x)$, $a^1 = a^2 = 1 \text{ s}^{-1}$, $\Delta = 600$, $V_{\text{Rx}} = V_{\text{Tx}} = V_{\text{vox}} = 10^{-6}$, $N = 100$, $D = 40 \times 10^{-9} \text{ m}^2/\text{s}$.

c) Phase C: In the third phase, the system is again modeled as a single container with $S_2 \rightarrow S_1$ and no diffusion. As in Phase A, the evolution of the concentrations $u_{C,2}$ is governed via (20), with $c_{C,2}$ in place of $c_{A,1}$ and initial conditions given by $u_{C,2}^0 = \Delta V_{\text{Rx}}/(NV_{\text{vox}})$ (due to spatial homogeneity in Phase B) and $u_{C,1}^0 = 0$. Hence,

$$u_{C,2}(t) = \frac{\Delta V_{\text{Rx}}}{(NV_{\text{vox}})} e^{-at}. \quad (26)$$

Note that, as discussed in Section III, the expected number of molecules in the receiver in equilibrium is $\mu_r = \frac{\Delta V_{\text{Rx}}}{NV_{\text{vox}} + 2V_{\text{Rx}}}$. The required time t_C to decrease from $\Delta V_{\text{Rx}}/(NV_{\text{vox}})$ to $\frac{\Delta V_{\text{Rx}}}{NV_{\text{vox}} + 2V_{\text{Rx}}}$ can be obtained by using (26) as

$$t_C = -\frac{1}{a^2} \log \left(\frac{NV_{\text{vox}}}{NV_{\text{vox}} + 2V_{\text{Rx}}} \right). \quad (27)$$

Let, $t_r = t_A + t_B$ and $t_d = t_C$ denote the required time to approach equilibrium. A useful heuristic for the required time to approach equilibrium is then given by

$$t^* = t_r + t_d, \quad (28)$$

which is plotted in Fig. 5 and evaluated for different parameters in Table III. In the table, $D_1(x) = D_2(x) = D$, $\epsilon = 10^{-3}$, $r = NV_{\text{vox}}/V_{\text{Rx}}$. The time t_{eq} corresponds to when the solution to (17) is first within ϵ of the equilibrium concentration. In order to calculate the t_{eq} , the system (17) is solved numerically.

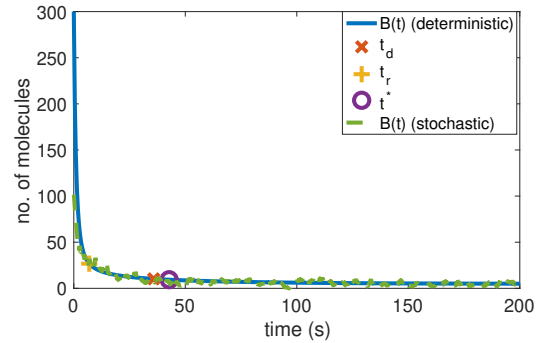


Fig. 5: Value of t^* for $D = 80 \times 10^{-11}$, $r = 60$, $a^1 = a^2 = a = 1$.

B. Optimizing the Threshold for Low Memory Detection

A key parameter for implementing the low memory detection scheme in Section III is the decision threshold. This

TABLE III: Sampling Time Heuristic t_{eq} for $\epsilon = 0.01$.

Parameters	t_B	$t_A + t_C$	t^*	t_{eq}
$D = 80 \times 10^{-9} \text{ m}^2/\text{s}, r = 60, a = 0.1 \text{ s}^{-1}$	0.3 s	74.3 s	74.6 s	80.1 s
$D = 80 \times 10^{-10} \text{ m}^2/\text{s}, r = 60, a = 0.1 \text{ s}^{-1}$	3.6 s	74.3 s	77.9 s	82 s
$D = 80 \times 10^{-11} \text{ m}^2/\text{s}, r = 60, a = 0.1 \text{ s}^{-1}$	36 s	74.3 s	110.3 s	118 s
$D = 80 \times 10^{-11} \text{ m}^2/\text{s}, r = 60, a = 1 \text{ s}^{-1}$	36 s	7.4 s	43.4 s	50.9 s
$D = 80 \times 10^{-11} \text{ m}^2/\text{s}, r = 100, a = 1 \text{ s}^{-1}$	99.4 s	7.4 s	106.8 s	114 s

parameter can be obtained by minimizing the probability of error, defined by

$$P_e^{n,m}(\tau) = \frac{1}{2} (\Pr(R(n) > \tau | s_n = 0) + \Pr(R(n) \leq \tau | s_n = 1)), \quad (29)$$

where n is the symbol index and m is the number of previously transmitter symbols corresponding to bit 1. This probability of error is evaluated in Proposition 1.

Proposition 1. *Assume that the previous $n - 1$ symbols have been correctly decoded, with m transmissions of bit 1. Then, under Assertion 1, the low memory detector in (13) has a probability of error for the n -th symbol given by*

$$P_e^{n,m}(\tau) = 0.5 \left(1 - Q \left(\frac{\tau - \mu_r}{\sqrt{(m+1)\mu_r + m\mu_r}} \right) \right) + 0.5Q \left(\frac{\tau}{\sqrt{2m\mu_r}} \right), \quad (30)$$

where $Q(x) = \int_x^\infty \frac{1}{\sqrt{2\pi}} \exp(-\frac{z^2}{2}) dz$, $x \in \mathbb{R}$.

Proposition 1 follows immediately from the Gaussian statistics in Assertion 1. Note that it is necessary to index $P_e^{n,m}$ by n and m due to the fact that the receiver observation statistics vary as n and m increase. As such, the optimal threshold also depends in general on n and m .

To proceed, we note that the derivative of $P_e^{n,m}(\tau)$ is given by

$$\frac{dP_e^{(n,m)}}{d\tau} = \frac{1}{\sqrt{2\pi(2m+1)\mu_r}} \exp\left(-\frac{(\tau - \mu_r)^2}{2(2m+1)\mu_r}\right) - \frac{1}{\sqrt{4\pi m\mu_r}} \exp\left(-\frac{\tau^2}{4m\mu_r}\right).$$

Therefore, for large m ,

$$\frac{dP_e^{(n,m)}}{d\tau} \approx -\frac{1}{\sqrt{4\pi m\mu_r}} \exp\left(-\frac{\tau^2}{4m\mu_r}\right) + \frac{1}{\sqrt{4\pi m\mu_r}} \exp\left(-\frac{(\tau - \mu_r)^2}{4m\mu_r}\right).$$

The threshold minimizing the probability of error for large m can then be well-approximated by

$$\tau^* = \frac{\mu_r}{2}. \quad (31)$$

We remark for a sufficiently large number of transmissions, even if some symbols have been incorrectly decoded, τ^* in (31) is a good approximation for the optimal threshold for the low memory detector.

C. Container Volume Estimation

Key parameters in equilibrium signaling are the relative volumes of the transmitter and receiver with respect to the total container volume. For applications *in vitro*, for example, the total volume the container and hence the relative volumes of the transmitter and receiver may not be known *a priori*. This is due to the fact that the exact environment of the molecular communication system may be complex or time varying. As such, it is highly desirable to estimate the container volume.

Unlike more detailed features of the container—which are required to optimize decisions in classical CSK—estimating the container volume is straightforward. Suppose that K transmissions of Δ molecules of S_1 , corresponding to K time slots, are allocated to volume estimation. Under Assertion 1, the observations x_1, \dots, x_K of the quantity of S_1 near equilibrium are independent with known Gaussian statistics. In particular, the variance of sample k is then given by $k\mu_r$, where μ_r is given by (7).

Under Assertion 1, the observations are Gaussian and therefore the maximum likelihood estimator $\hat{\mu}_r$ for μ_r is the solution to

$$\hat{\mu}_r = \arg \max_{\mu_r} \prod_{k=1}^K \frac{1}{\sqrt{2\pi k\mu_r}} \exp\left(-\frac{(x_k - k\mu_r)^2}{2k\mu_r}\right), \quad (32)$$

which admits a solution satisfying

$$\sum_{k=1}^K \frac{k}{2} + \sum_{k=1}^K \frac{1}{2\hat{\mu}_r} + \frac{1}{2} \sum_{k=1}^K \frac{x_k^2}{2k\hat{\mu}_r^2} = 0. \quad (33)$$

While the objective in (32) is in general non-convex, it is twice differentiable and therefore it is straightforward to verify numerically which of the solutions corresponds to a maximum.

An expression for the relationship between μ_r and the total volume of the container NV_{vox} is given in (7). Using this relationship, the estimator for the volume of the container NV_{vox} is given by

$$NV_{\text{vox}} = \frac{\Delta V_{\text{Rx}} - \hat{\mu}_r \frac{a^1}{a^2} (V_{\text{Tx}} + V_{\text{Rx}})}{\hat{\mu}_r}. \quad (34)$$

Fig. 6 shows the impact of increasing the number of samples on the normalized mean-square error (NMSE). Observe that using (33), it is possible to estimate the volume of the container with low NMSE even for small numbers of samples and regardless of the true value of μ_r .

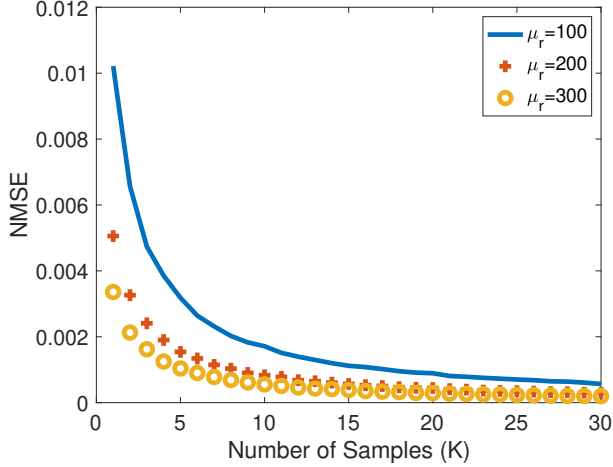


Fig. 6: Plot of NMSE for varying numbers of samples and μ_r .

VI. NUMERICAL RESULTS

A. Performance Evaluation

In this section, we study the performance of the proposed equilibrium signaling scheme via particle-based simulations. Both the near-optimal and low memory schemes are compared, along with a classical CSK scheme. These comparisons are based on transmissions of $n = 1000$ bits. Since the channel is non-stationary, the performance is evaluated in terms of the average number of errors in the sequence of n bits. More formally, let E_i be the error random variable for bit i in the sequence; that is

$$E_i = \begin{cases} 1 & \hat{s}_i \neq s_i, \\ 0 & \hat{s}_i = s_i, \end{cases} \quad (35)$$

where \hat{s}_i is the estimate of the transmitted bit s_i . Then, the average probability of error is defined as

$$P_{ave} = \mathbb{E} \left[\frac{1}{n} \sum_{i=1}^n E_i \right]. \quad (36)$$

In order to estimate P_{ave} , 10000 iterations of the transmission of n bits are simulated.

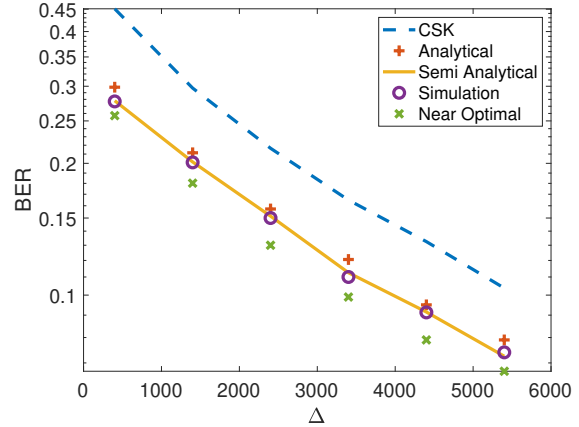
The parameters used in the simulations are: $a^1 = a^2 = 1s^{-1}$; $D_1 = D_2 = 80 \times 10^{-11} m^2/s$; $T_s = t^*$ given in (28); and $V_{Rx} = V_{Tx}$. We remark that very similar results are obtained with different choices of a^1, a^2, D_1, D_2 as long as the ratio a^1/a^2 remains constant. This is due to the fact that μ_r only depends on the ratio and not the precise values of a^1 and a^2 .

In the numerical results, five scenarios are considered by using channel in Fig. 2a:

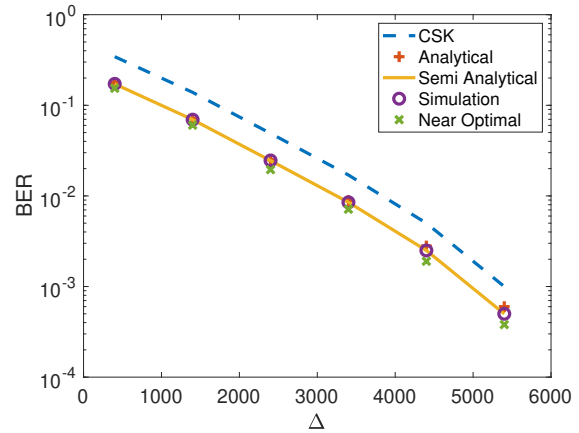
- (i) *Near-optimal detection scheme*: The average probability of error for Viterbi-based detection scheme developed in Sec. III-A is obtained via particle-based simulations. In particular, the kinetics arising from the RDME model are simulated using the next reaction algorithm [30].
- (ii) *Low memory detection scheme*: The average probability of error for the low memory detection scheme developed

in Sec. III-B is obtained via particle-based simulations in the same manner as for the near-optimal scheme.

- (iii) *Semi-analytical evaluation*: For the low memory detection scheme developed in Sec. III-B, the observations in the receiver are simulated based on Assertion 1.
- (iv) *Analytical evaluation*: For the low memory detection scheme developed in Sec. III-B, the probability of error is approximated by the expression in Proposition 1.
- (v) *Classical CSK*: The average probability of error for the classical CSK scheme—where only a single molecule is employed (see, for example, [32])—is obtained via particle-based simulations as for the near-optimal scheme. The sampling time for the classical CSK is also chosen as t^* with observations drawn from S_2 , which is necessary due to limitations of the biological oscillator needed to implement sampling.



(a) $V_{Rx}/(NV_{vox}) = 0.01$.



(b) $V_{Rx}/(NV_{vox}) = 0.1$.

Fig. 7: BER performance for different $V_{Rx}/(NV_{vox})$.

Fig. 7 plots the average probability of error for varying quantities of emitted molecules Δ , in each of the five scenarios and with varying receiver and transmitter volumes. As expected, the near-optimal scheme based on the Viterbi algorithm outperforms the low memory scheme. The performance gains depend on the relative volume of the receiver, ranging from approximately 300 molecules in the case where

$V_{RX}/(NV_{VOX}) = 0.05$. In general, this suggests a tradeoff between the complexity of the receiver and available energy in the transmitter.

Fig. 7 also shows that for the low memory scheme, the semi-analytical and analytical models well approximate the results from particle-based simulations. This provides further evidence for the validity of Assertion 1 and also Proposition 1.

Finally, Fig. 7 shows a dramatic performance gain using equilibrium signaling over classical CSK under the sampling time constraint. To gain intuition into why this gain arises, observe that near equilibrium the average number of molecules observed in the receiver under classical CSK will be $\Delta \frac{V_{RX}}{NV_{VOX}}$. On the other hand, the equilibrium signaling scheme yields on average the quantity μ_r given by (7). In any scenario where the number of voxels comprising the channel is greater than zero, $\mu_r > \Delta \frac{V_{RX}}{NV_{VOX}}$, which results in performance gains.

We remark that the gain of equilibrium signaling over classical CSK may not be present if the sampling time is optimized for classical CSK. However, realistic biological circuits place strong constraints on sampling [20] and therefore such a constraint on the sampling time may be unavoidable.

B. Robustness to Uncertainties in System Geometry

A key motivation for equilibrium signaling is that the scheme only relies on knowledge of the container volume. This stands in stark contrast to classical CSK schemes, which require knowledge of the distance between the transmitter and the receiver, as well as the shape of the container.

The problem of estimating the distance between a transmitter and receiver has been investigated in [33], [34]. However, in biological environments, the relative locations of the transmitter and receiver may change relatively often. As a consequence, the estimation procedure may need to be repeated regularly, which leads to additional energy expenditure.

If the distance is not perfectly known, then there is a degradation in performance. This is illustrated in Fig. 8 for the conventional CSK presented in [9], where small errors in distance estimation can lead to significant performance losses in terms of the probability of error.

On the other hand, our proposed equilibrium schemes are not affected by errors in distance estimation or even the shape of the container. For example, it is straightforward to optimize the receiver for both of the scenarios in Fig. 1, as long as the relative volumes of the transmitter and the receiver are known.

As noted in Sec. V-C, there exists a simple strategy for estimating the container volume. With a sufficient number of samples, a very low volume estimation error can be obtained. It is clear that, any error in the volume estimate will lead to performance losses, which is illustrated in Fig. 9. Observe that, even for the highest estimation error on μ_r (from Fig. 6, one can observe that for small K , the maximum NMSE is around 0.01) there is not a significant performance loss in terms of BER.

VII. CONCLUSION

A key challenge for molecular communications, particularly in biological environments, is uncertainty in the geometry of

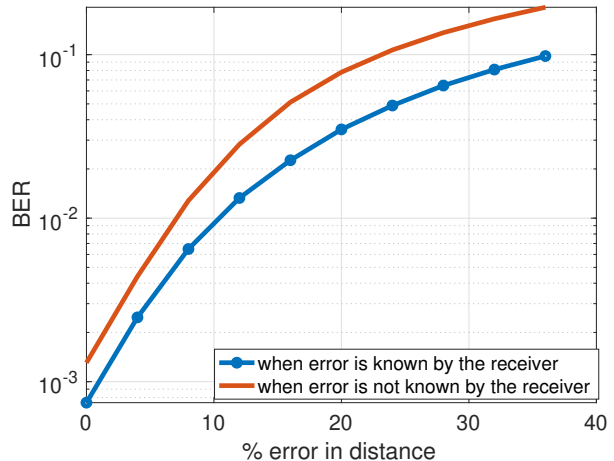


Fig. 8: BER vs error in distance for classical CSK [9]. Parameters: $D = 80 \times 10^{-12} \text{ m}^2/\text{s}$, the correct distance is 10^{-5} m , $T_s = 0.25 \text{ s}$.

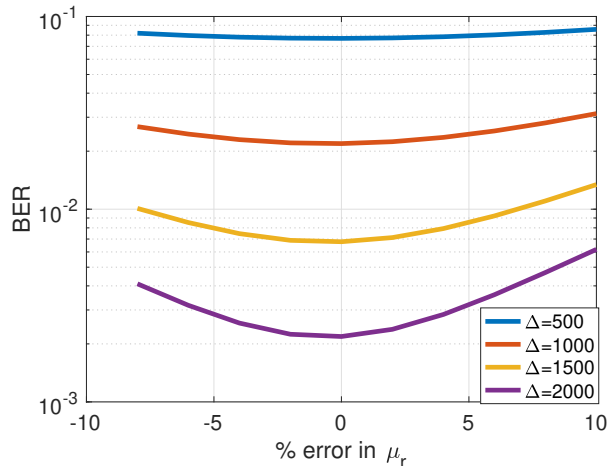


Fig. 9: BER vs estimation error in μ_r .

the environment. This uncertainty may take the form of the shape of the environment, or the distance between the transmitter and the receiver. As it is not necessarily straightforward to estimate parameters of the environment and schemes such as classical CSK are not robust to changes in the geometry, it is highly desirable to develop schemes that are in fact robust.

In this paper, we proposed equilibrium signaling, which only requires knowledge of the container volume in order to develop near-optimal detection schemes. This robustness comes at the cost of large sampling times; however, it is necessary in some applications to exploit biological oscillators in order to obtain samples. As such, the requirement of long sampling periods may in fact be a realistic system constraint.

This work raises several new questions. From an engineering perspective, it is desirable to develop complete biological circuits in order to implement coding and detection tailored to equilibrium signaling. Another direction is to establish a rigorous characterization of the deterministic limit used to obtain the statistics for the receiver observations.

REFERENCES

- [1] H. Arjmandi, A. Gohari, M. Kenari, and F. Bateni, "Diffusion-based nanonetworking: a new modulation technique and performance analysis," *IEEE Communications Letters*, vol. 17, no. 4, pp. 645–648, 2013.
- [2] B. Atakan and O. Akan, "On channel capacity and error compensation in molecular communication," *Transactions on Computational Systems Biology X*, vol. 10, pp. 59–80, 2008.
- [3] —, "Deterministic capacity of information flow in molecular nanonetworks," *Nano Communication Networks*, vol. 1, no. 1, pp. 31–42, 2010.
- [4] M. Mahfuz, D. Makrakis, and H. Mouftah, "Spatiotemporal distribution and modulation schemes for concentration-encoded medium-to-long range molecular communications," in *25th Biennial Symp. Commun.*, 2010.
- [5] I. Llatser, A. Cabellos-Aparicio, M. Pierobon, and E. Alarcon, "Detection techniques for diffusion-based molecular communication," *IEEE Journal on Selected Areas in Communications*, vol. 31, no. 12, pp. 726–734, 2013.
- [6] N.-R. Kim and C.-B. Chae, "Novel modulation techniques using isomers as messenger molecules for nano communication networks via diffusion," *IEEE Journal of Selected Areas in Communications*, vol. 31, no. 12, pp. 847–856, 2013.
- [7] M. Mahfuz, D. Makrakis, and H. Mouftah, "Concentration-encoded subdiffusive molecular communication: theory, channel characteristics, and optimum signal detection," *IEEE Transactions on NanoBioscience*, vol. 15, no. 6, pp. 533–548, 2016.
- [8] —, "A comprehensive study of sampling-based optimum signal detection in concentration-encoded molecular communication," *IEEE Transactions on NanoBioscience*, vol. 13, no. 3, pp. 208–222, 2014.
- [9] M. Kuran, H. Yilmaz, T. Tugcu, and I. Akyildiz, "Modulation techniques for communication via diffusion in nanonetworks," in *IEEE International Conference on Communications (ICC)*, 2011.
- [10] —, "Interference effects on modulation techniques in diffusion based nanonetworks," *Nano Communication Networks*, vol. 3, no. 1, pp. 65–73, 2012.
- [11] H. B. Yilmaz, A. C. Heren, T. Tugcu, and C.-B. Chae, "Three-dimensional channel characteristics for molecular communications with an absorbing receiver," *IEEE Communications Letters*, vol. 18, no. 6, pp. 929–932, 2014.
- [12] H. Shahmohammadian, G. Messier, and S. Magierowski, "Optimum receiver for molecule shift keying modulation in diffusion-based molecular communication channels," *Nano Communication Networks*, vol. 3, no. 3, pp. 183–195, 2012.
- [13] A. Hamdan and C. Chou, "Generalized solution for the demodulation of reaction shift keying signals in molecular communication networks," *IEEE Transactions on Communications*, vol. 65, no. 2, pp. 715–727, 2016.
- [14] M. Cuchiara, A. Allen, T. Chen, J. Miller, and J. West, "Multilayer microfluidic PEGDA hydrogels," *Biomaterials*, vol. 31, pp. 5491–5497, 2010.
- [15] C. Chen, B. Mehl, A. Munshi, A. Townsend, D. Spence, and R. Martin, "3D-printed microfluidic devices: fabrication, advantages and limitations—a mini review," *Analytical Methods*, vol. 8, no. 31, pp. 6005–6012, 2016.
- [16] S. Schindera, P. Mehwald, D. Sahn, and D. Kececioglu, "Accuracy of real-time three-dimensional echocardiography for quantifying right ventricular volume," *Journal of Ultrasound in Medicine*, vol. 21, no. 10, pp. 1069–1075, 2002.
- [17] L. Desvillettes, K. Fellner, and B. Tang, "Trend to equilibrium for reaction-diffusion systems arising from complex balanced chemical reaction networks," *SIAM Journal on Mathematical Analysis*, vol. 49, no. 4, pp. 2666–2709, 2017.
- [18] V. Jamali, N. Farsad, R. Schober, and A. Goldsmith, "Diffusive molecular communications with reactive molecules: channel modeling and signal design," *IEEE Transactions on Molecular, Biological and Multi-Scale Communications*, vol. 4, no. 3, pp. 171–188, 2018.
- [19] A. Noel, K. Cheung, and R. Schober, "Improving receiver performance of diffusive molecular communication with enzymes," *IEEE Transactions on NanoBioscience*, vol. 13, no. 1, pp. 31–43, 2014.
- [20] E. Shitiri, A. Vasilakos, and H. Cho, "Biological oscillators in nanonetworks—opportunities and challenges," *Sensors*, vol. 18, no. 5, 2018.
- [21] D. Soloveichik, G. Seelig, and E. Winfree, "DNA as a universal substrate for chemical kinetics," *Proceedings of the National Academy of Sciences*, vol. 107, no. 12, pp. 5393–5398, 2010.
- [22] S. Isaacson, "The reaction-diffusion master equation as an asymptotic approximation of diffusion to a small target," *SIAM Journal on Applied Mathematics*, vol. 70, no. 1, pp. 77–111, 2009.
- [23] C. Chou, "Extended master equation models for molecular communication networks," *IEEE Transactions on NanoBioscience*, vol. 12, no. 2, pp. 79–92, 2013.
- [24] S. Ethier and T. Kurtz, *Markov Processes: Characterization and Convergence*. John Wiley & Sons, 2009.
- [25] D. Gillespie, "The chemical Langevin equation," *The Journal of Chemical Physics*, vol. 113, no. 1, pp. 297–306, 2000.
- [26] L. Cardelli, M. Kwiatkowska, and L. Laurenti, "Stochastic analysis of chemical reaction networks using linear noise approximation," *Biosystems*, vol. 149, pp. 26–33, 2016.
- [27] T. Kurtz, "The relationship between stochastic and deterministic models for chemical reactions," *The Journal of Chemical Physics*, vol. 57, no. 7, pp. 2976–2978, 1972.
- [28] L. Arnold and M. Theodosoplu, "Deterministic limit of the stochastic model of chemical reactions with diffusion," *Advances in Applied Probability*, vol. 12, no. 2, pp. 367–379, 1980.
- [29] M. Egan, B. Q. Tang, and B. C. Akdeniz, "On the input-output relationship for molecular communications in general first-order chemical reaction-diffusion systems," in *Proceedings of the Sixth Annual ACM International Conference on Nanoscale Computing and Communication*. ACM, 2019, p. 21.
- [30] J. Elf, A. Donic, and M. Ehrenberg, "Mesoscopic reaction-diffusion in intracellular signaling," in *Fluctuations and noise in biological, biophysical, and biomedical systems*, vol. 5110. International Society for Optics and Photonics, 2003, pp. 114–125.
- [31] F. Massey, "The Kolmogorov-Smirnov test for goodness of fit," *Journal of the American statistical Association*, vol. 46, no. 253, pp. 68–78, 1951.
- [32] H. Arjmandi, M. Zoofaghari, and A. Noel, "Diffusive molecular communication in a biological spherical environment with partially absorbing boundary," *arXiv preprint arXiv:1810.02657*, 2018.
- [33] M. Turan, B. C. Akdeniz, M. Ş. Kuran, H. B. Yilmaz, I. Demirkol, A. E. Pusane, and T. Tugcu, "Transmitter localization in vessel-like diffusive channels using ring-shaped molecular receivers," *IEEE Communications Letters*, vol. 22, no. 12, pp. 2511–2514, 2018.
- [34] A. Noel, K. C. Cheung, and R. Schober, "Joint channel parameter estimation via diffusive molecular communication," *IEEE Transactions on Molecular, Biological and Multi-Scale Communications*, vol. 1, no. 1, pp. 4–17, 2015.